Journal of Marine Science and Technology

Volume 24 | Issue 6 Article 14

AN INCREASED REMOTE SENSING OBSERVATION BY GOCI DAILY COMPOSITE IMAGE

Hyun Yang
Korea Institute of Ocean Science and Technology, Haean-no, Ansan, Korea

Wonkook Kim
Korea Institute of Ocean Science and Technology, Haean-no, Ansan, Korea

Kwangseok Kim
Korea Institute of Ocean Science and Technology, Haean-no, Ansan, Korea

Young-Je Park
Korea Institute of Ocean Science and Technology, Haean-no, Ansan, Korea.

Hee-Jeong Han
Korea Institute of Ocean Science and Technology, Haean-no, Ansan, Korea

See next page for additional authors

AN INCREASED REMOTE SENSING OBSERVATION BY GOCI DAILY COMPOSITE IMAGE

Acknowledgements

This research was supported by the “Research for applications of Geostationary Ocean Color Imager (GOCI)” and the “Development of the integrated data processing system for GOCI-II” funded by the Ministry of Ocean and Fisheries, Korea. This research was also supported by the “Operation in Korea Ocean Satellite Center” funded by the Korea Institute of Ocean Science and Technology (KIOST).

Authors

Hyun Yang, Wonkook Kim, Kwangseok Kim, Young-Je Park, Hee-Jeong Han, and Joo-Hyung Ryu

Journal of Marine Science and Technology, Vol. 24, No. 6, pp. 1161-1170 (2016)
DOI: 10.6119/JMST-016-1026-5

AN INCREASED REMOTE SENSING OBSERVATION BY GOCI DAILY COMPOSITE IMAGE

Hyun Yang, Wonkook Kim, Kwangseok Kim, Young-Je Park,
Hee-Jeong Han, and Joo-Hyung Ryu

Key words: Geostationary Ocean Color Imager, GOCI, daily composite, ocean color.

ABSTRACT

Opaque masses (e.g., cloud and haze) are the main obstacles interrupting remote observations of ocean color using optical sensors. We performed a statistical analysis for 1 year of ocean color data derived from the Geostationary Ocean Color Imager (GOCI), which performs eight observations per day. We discovered that the valid ranges of the data vary depending on the local times and the seasonal characteristics and are related to the pattern of solar altitudes to a certain degree. Here, it is shown that multiple ocean color scenes observed on a given day can be merged to recover the contaminated areas. However, merging multiple ocean color scenes from heterogeneous sensors (e.g., MODIS, SeaWiFS, and MERIS) for a given day takes considerable effort. In contrast, multiple scenes from a single sensor such as GOCI can be merged with a relatively simple approach such as averaging. Here, we focus on how much unavailable data can be recovered quantitatively in a given day by merging multiple scenes from GOCI. To this end, a large data set composed of GOCI scenes from January 2012 to December 2012 was used. The results demonstrate that ocean color availability in a composite scene merged from eight multiple GOCI scenes could be expanded by about 2.54 times relative to a single scene.

I. INTRODUCTION

In optical and thermal remote sensing, one of the main obstacles in the ocean color observation is opaque masses in the atmosphere such as cloud, haze, and sea fog (Cihlar and Howarth, 1994; Wang and Shi, 2006). The loss of the remote sensing data due to the opaque masses make it difficult to analyze the features of ocean color such as patterns of continuous oceanic patches or eddies. To facilitate data analysis, the missing data should be accounted for. One way to compensate for missing data is to merge multiple scenes (Campbell and Hooker, 1995). In the case of ocean color remote sensing, research aimed at investigating and improving the amount of available data has also been conducted. Traditionally, such research can be classified into two categories: (1) the use of numeric models or optimal interpolations (He et al., 2003; Alvera-Azcarate et al., 2007) and (2) the merging of multiple scenes (Pottier et al., 2006; Roy et al., 2006; Maritorena et al., 2010).

The optimal interpolation scheme based upon the correlation model was developed by He et al. (2003) to improve the availability of sea surface temperature data derived from Advanced Very High Resolution Radiometer (AVHRR) scenes. The empirical scheme based upon the Data Interpolating Empirical Orthogonal Functions (DINEOF) was proposed by Alvera-Azcarate et al. (2007) to recover the lost ocean color data in the area covered with clouds. Using this scheme, they reconstructed the lost parts in the scenes which contain the sea surface temperature derived from AVHRR and the chlorophyll concentration derived from Moderate Resolution Imaging Spectroradiometer (MODIS).

The schemes using the numeric models tend to exploit only one satellite scene. These schemes enable that the results can be more distorted but the satellite scenes can be simply collected. The merging methods, on the other hand, exploit the multiple scenes. These methods tend to be that the results can be more accurate while it takes effort to collect and combine the multiple satellite scenes. Pottier et al. (2006) evaluated and compared two methods of ocean color data merging (i.e., the weighted averaging and the objective analysis) with dataset which involves chlorophyll concentration from the Sea-viewing Wide Field-of-view Sensor (SeaWiFS), and MODIS. They concluded that the weighted averaging method is more straightforward but the objective analysis method is more accurate. Roy et al. (2006) studied and analyzed the data set which contains the cloud occurrence probabilities produced by MODIS in order to examine the global impact of cloud. They also composed the MODIS scenes within a few days for the purpose of gaining the more available

Paper submitted 05/27/16; revised 06/16/16; accepted 10/31/16. *Author for correspondence: Joo-Hyung Ryu (e-mail: jhryu@kiost.ac.kr).*
Korea Institute of Ocean Science and Technology, Haean-no, Ansan, Korea.

data. Maritorena et al. (2010) used a semi-analytical model and the observations of normalized water-leaving radiance in order to merge the multiple scenes from the SeaWiFS, MODIS, and Medium Resolution Imaging Spectrometer (MERIS).

In existing approaches, where the goal is to improve the availability of ocean color information on a given day by merging multiple ocean color scenes (Pottier et al., 2006; Maritorena et al., 2010), most have exploited scenes merged from heterogeneous sensors (e.g., MODIS (Esaias et al., 1998), SeaWiFS (McClain et al., 2004), MERIS (Rast et al., 1999) etc. These sensors, which operate in polar orbits, can obtain just one or two scenes. For polar orbit platforms, ocean color scenes derived from heterogeneous sensors are therefore merged to improve the availability on a given day. In this environment, several differences in key parameters (e.g., the intensity of radiation, the ground sampling distance, and the polar orbit path) that originate from the heterogeneous sensors make it difficult to merge the scenes (Maritorena and Siegel, 2005).

In this study, in contrast, we exploited multiple ocean color scenes derived from a single sensor, the Geostationary Ocean Color Imager (GOCI) (Han et al., 2010; Ryu et al., 2012). GOCI is the world's first satellite remote sensor operating in a geostationary orbit that captures ocean color (Kang et al., 2004; Cho et al., 2010). It produces ocean color scenes in the Northeast Asian region at a high temporal resolution of 1 hour, eight times a day, and thus can provide observations of sensitive changes in the oceanic environment (Choi et al., 2012, Yang et al., 2014, and Yang et al., 2016). In particular, the available coverage on a given day can be expanded by merging the eight hourly scenes produced by GOCI. The composition of GOCI scenes can be obtained through averaging (Yang et al., 2012). In this paper, we focus on the quantitative improvement of data availability using eight GOCI observations. Additionally, the changes in the amount of available data with local time and month series were investigated. Finally, we were able to obtain a wider range of available ocean color data (i.e., chlorophyll concentration) by merging eight GOCI observations.

The rest of this paper is organized as follows. Section 2 describes the dataset used in our evaluations and experiments. A method to calculate the available area and the results of our experiments are presented in Section 3. In Section 4, we offer conclusions and suggestions for further studies.

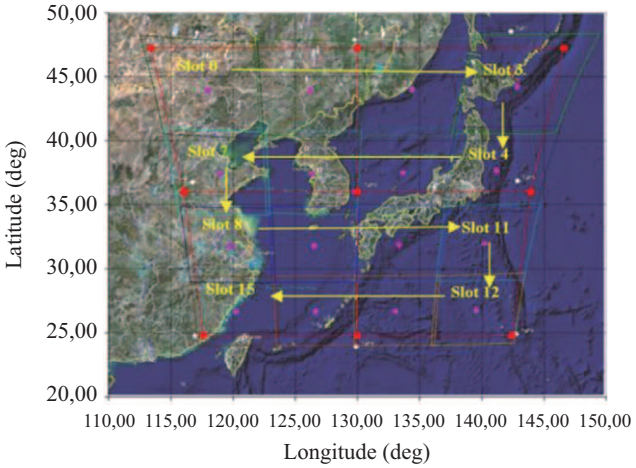

Fig. 1. GOCI raw data is composed of 16 (4 × 4) slots of which size is equavalent to the GOCI IFOV (Ryu et al., 2012).

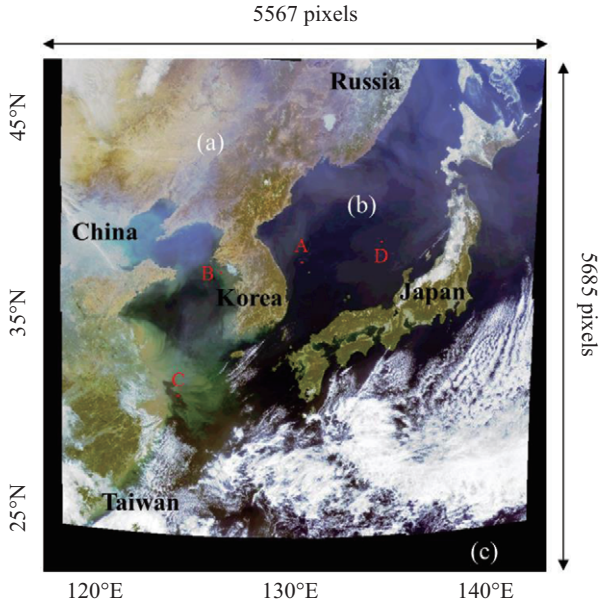

Fig. 2. Colored image and geographical components of the geometrically corrected GOCI level 1 scene. Korea, China, Japan, Russia, and Taiwan are covered in a GOCI level 1 scene. The geographical composition of the GOCI level 1 scene is divided into land (a), ocean (b), and the edge frame (c). The location A indicates a sea area where oceanic eddies are formed frequently, B is a region that has a semidiurnal tide, C indicates a region that has extremely turbid water, and D is a relatively clear sea area.

II. DATA

GOCI is one of the three payloads on the Communication, Ocean and Meteorological Satellite (COMS), which was successfully launched at the Kourou Space Center in French Guiana by the Ariane 5 Launch Vehicle on 27 June 2010. GOCI was jointly developed by the EADS Astrium in France and the Korea Aerospace Research Institute (KARI), and follows user requirements from the Korea Institute of Ocean Science and Technology (KIOST).

GOCI is equipped with six visible bands and two near-infrared bands. The centers of the bandwidths are 412, 443, 490, 555, 660, and 680 nanometers for the visible band and 745 and 865 nanometers for the near-infrared band. The observation coverage and the ground sampling distance (GSD) of GOCI are a 2,500 × 2,500 km^2 centered at 36°N and 130°E and 0.5 km, respectively. GOCI was designed to capture and transmit scenes every hour, eight times a day between 9:30 and 16:30 local time (Han et al., 2010; Ryu et al., 2012).

A raw scene observed by GOCI is composed of 16 (4 × 4) slots (Fig. 1). The instantaneous field of view (IFOV) of GOCI

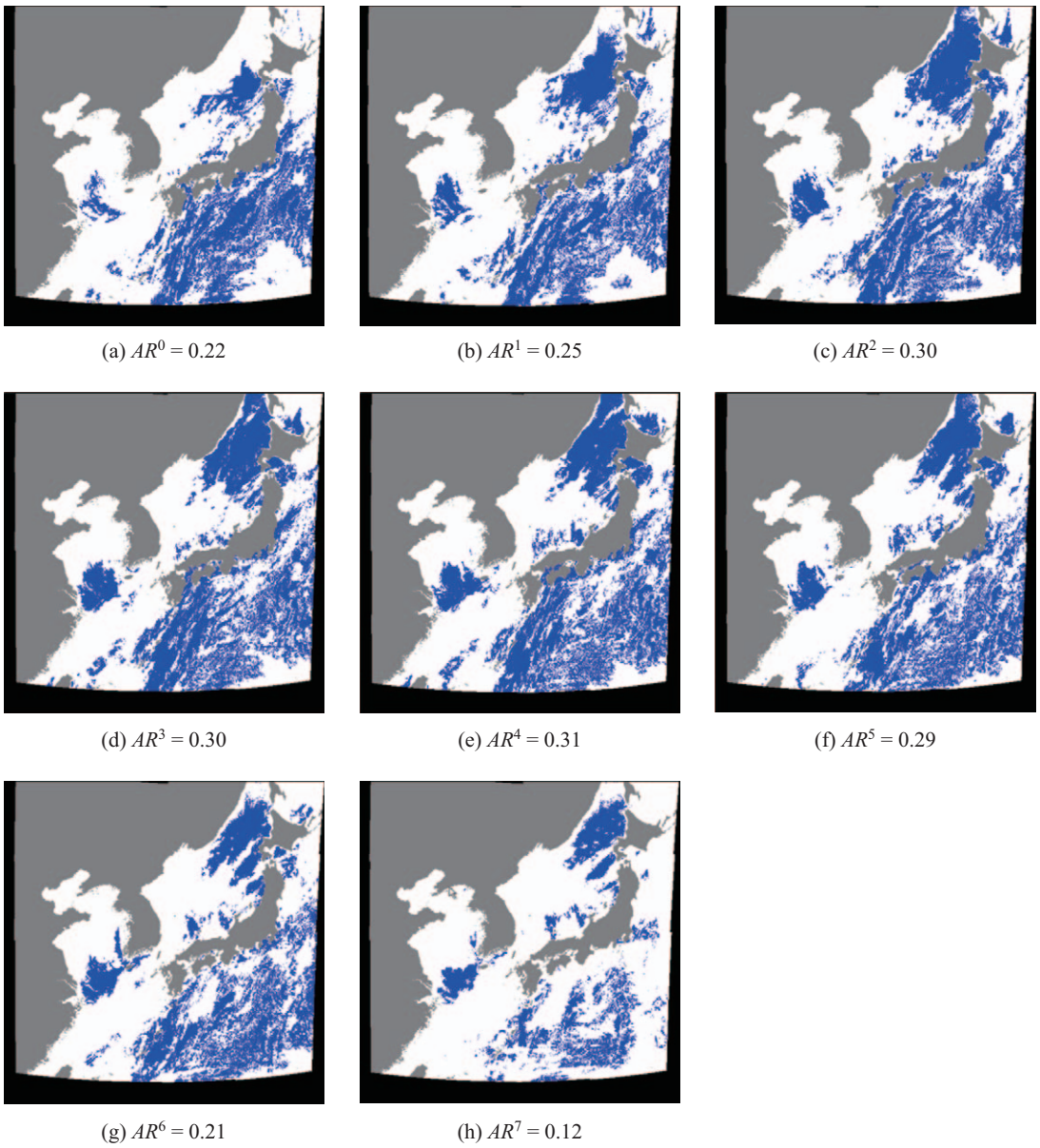

(a) $AR^0 = 0.22$ (b) $AR^1 = 0.25$ (c) $AR^2 = 0.30$

(d) $AR^3 = 0.30$ (e) $AR^4 = 0.31$ (f) $AR^5 = 0.29$

(g) $AR^6 = 0.21$ (h) $AR^7 = 0.12$

Fig. 3. Changes in the available coverage and available rate, AR^i, i = (0, 1, …, 7), at 9:30 (a), 10:30 (b), 11:30 (c), 12:30 (d), 13:30 (e), 14:30 (f), 15:30 (g), and 16:30 (h) local time on 30 August 2012. In these scenes, the blue/white parts are ocean areas with available/unavailable data. The average from AR^1 to AR^7 is about 0.27.

corresponds to the field of view (FOV) of the slot area due to GOCI's two-dimensional complementary metal-oxide semiconductor (CMOS) and 1,413 × 1,430 effective-pixel arrays (Cho et al., 2010). All scenes geometrically corrected from the raw scenes consist of 31,648,395 pixels (5,567 width and 5,685 height; Ryu et al., 2012). We refer to the geometrically corrected scene as a GOCI level 1 scene.

A GOCI level 1 scene can be divided into three components: the edge frame, the land, and the ocean area (Fig. 2). The edge-frame areas refer to invalid data produced in the process of geometrical correction, and the land areas denote the territories related to Korea, China, Japan, Russia, and Taiwan. This paper is concerned only with the ocean area. The average percentages of the edge-frame, land, and ocean areas are about 13%, 34%, and 53%, and the standard deviations of these values are 0.03%, 0.05%, and 0.08% in the GOCI level 1 scenes from January 2012 to December 2012. There was little change in those percentages because the GOCI always captures scenes of the geographically equivalent area due to its geostationary orbit.

The GOCI level 2 scenes such as the cloud mask, the chlorophyll concentration, the colored dissolved organic matter (CDOM), and the total suspended solid (TSS) can be derived from the GOCI level 1 scene by the GOCI Data Processing System (GDPS; Ryu et al., 2012). To achieve our goals, the

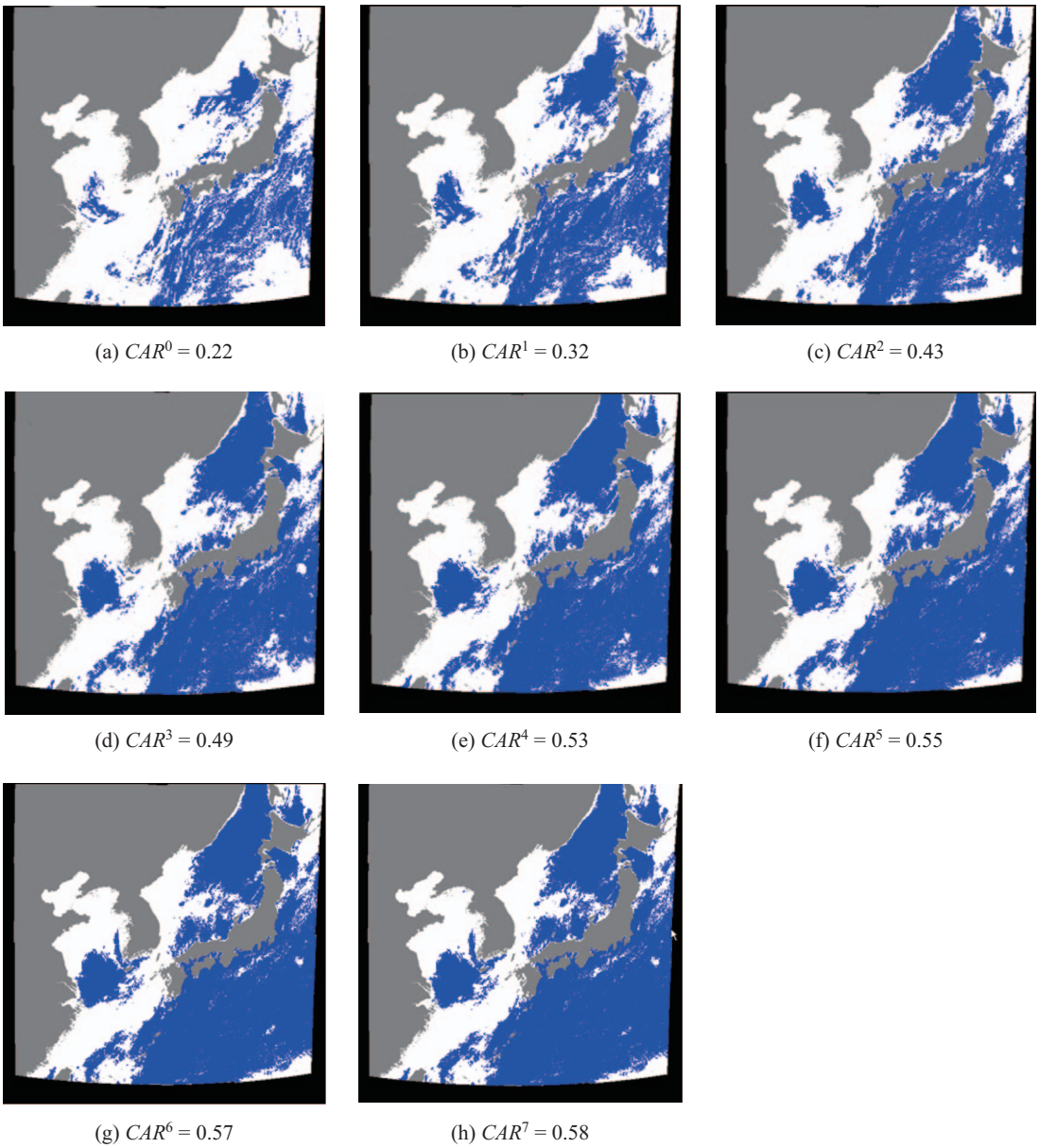

(a) $CAR^0 = 0.22$ (b) $CAR^1 = 0.32$ (c) $CAR^2 = 0.43$

(d) $CAR^3 = 0.49$ (e) $CAR^4 = 0.53$ (f) $CAR^5 = 0.55$

(g) $CAR^6 = 0.57$ (h) $CAR^7 = 0.58$

Fig. 4. Changes in the cumulative available rate, CAR^j, j = (0, 1, …, 7) at 9:30 (a), 9:30-10:30 (b), 9:30-11:30 (c), 9:30-12:30 (d), 9:30-13:30 (e), 9:30-14:30 (f), 9:30-15:30 (g), and 9:30-16:30 (h) local time on 30 August 2012. In these scenes, the blue/white parts are ocean areas with available/unavailable data. For example, CAR^3 (d) represents the cumulative available rate for the composite scene derived from four scenes between 9:30 and 12:30.

mass data are supported by the Korea Ocean Satellite Center (KOSC), which is the main operating agency of GOCI (http://kosc.kiost.ac). The data sizes of GOCI level 1 and 2 scenes are 966 megabytes (31,648,395 pixels per scene × 4 bytes per pixel × 8 bands) and 120 megabytes (31,648,395 pixels per scene × 4 bytes per pixel), respectively. In total, we used 3.2 terabytes of data from 1 January 2012 to 31 December 2012: (966 + 120 megabytes per scene) × 8 observation per day × 365 days.

III. METHODS AND RESULTS

In the GOCI level 2 scenes, the mask scene was exploited to investigate the rate of available data over the ocean area in the Northeast Asian region. As mentioned, the scenes were observed by GOCI at hourly intervals up to eight times every day; hence, the data array of a mask scene, M^i at index time i, for a given day is represented by

$$M^i = (m_0^i, m_1^i, \ldots, m_n^i), \; i = (0, 1, \ldots, 7)$$
$$m_x^i = \begin{cases} 0, & if\ rho\_s(865) > 0.028 \\ 1, & else \end{cases} \quad (1)$$

where n is the number of pixels corresponding to the ocean areas

in the mask scene, and i is the time index indicating when each scene is observed (Yang et al., 2012). Here, the time indices (0, 1, …, 7) indicate the local times (9:30, 10:30, …, 16:30). The values of m^i_x corresponding to the available and unavailable pixel data are 0 or 1. The availability of pixel data is determined by a cloud detection method of KOSC standard atmospheric correction algorithm, which regards data as unavailable when the value of reflectance at 865 nanometers (the near infrared band) [i.e., *rho_s*(*865*)] after Rayleigh correction is higher than 0.028 (Moon et al., 2012; Ahn et al., 2012). The available rate (*AR*) can be also determined by this algorithm. The AR^i in the scene observed at i index time for a given day can be defined by

$$AR^i = \frac{\sum_{k=0}^{n} m_k^i}{n} \quad (2).$$

Fig. 3 shows the changes in the available coverage and the AR^i, i = (0, 1, …, 7), at each hour on 30 August 2012. The distributions of the available coverage differ from scene to scene, and hence, the distributions vary with time. It is possible to improve the available area for a given day by composing multiple scenes.

We calculated the cumulative available rate (*CAR*), that is, the available rate of the composite scene from 0 to j index time on a given day, in order to validate improvement in the amount of available data using the eight GOCI observations. The CAR^j can be defined by

$$CAR^j = \frac{\sum_{k=0}^{n} \left\lfloor \frac{\sum_{i=0}^{j} m_k^i}{j+1} \right\rfloor}{n}, \; j = (0, 1, \ldots, 7) \quad (3)$$

where j is the time index when each scene is observed. The time indices (0, 1, …, 7) indicate the local times (9:30, 10:30, …, 16:30). The changes in CAR^j, j = (0, 1, …, 7) on 30 August 2012 are shown in Fig. 4.

The *AR* for the single scene at 9:30 is about 0.22. This available rate is improved by 2.23 times for CAR^3 = 0.49, which is the *CAR* for the composite scene derived from four scenes between 9:30 and 12:30 local time; it is improved by 2.64 times for CAR^7 = 0.58, which is the *CAR* for the composite scene derived from eight scenes between 9:30 and 16:30 local time. It is particularly interesting to note that the range of holes caused by unavailable data (white area) narrows, and the continuously available range (blue area) widens as the cumulative number of composite scenes is increased.

We also investigated how the coverage of composite scenes improved statistically. The results are shown in Fig. 5. The yearly averages of the *CAR* for GOCI data during 2012 increased continuously as the number of merged scenes increased. The

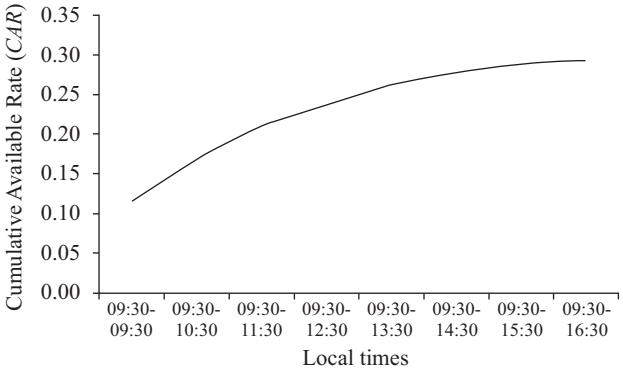

Fig. 5. Yearly *CAR* averages for GOCI data during 2012.

yearly average CAR^7 (= 0.293) for the composite scene derived from eight scenes from 9:30 to 16:30 was improved by about 2.54 times relative to the CAR^0 (= 0.115) for Similar to these results, Fig. 6 shows how the amount of available data improves with multiple GOCI observations. Here, the daily availability of GOCI data refers to the percentage of available observations of the eight observations during a day. It shows that the available coverage expands continuously as the number of merged observations is increased. From the figure, we can also see that certain areas are consistently available, whereas other areas are always unavailable. The consistently unavailable areas around coastal regions are closely related to our masking algorithm (i.e., the KOSC standard atmospheric correction algorithm) because extremely high turbidities on coastal regions obstruct the ocean color remote sensing (Ruddick et al., 2000). For consistently available areas, however, we propose that the results are caused by the seasonal characteristics for a given data set (i.e., GOCI data during August 2012).

IV. DISCUSSIONS AND CONCLUSIONS

In this paper, we focused on how the amount of available data can be increased by using eight GOCI observations. The experimental evaluation demonstrated that the availability of data was expanded by about 2.54 times in a composite scene derived by merging eight observations relative to a single scene. We also discovered that the availability in ocean color scenes around the Northeast Asian region is affected by changes in the local time and seasonal characteristics.

Unlike the case of merging ocean color scenes from heterogeneous sensors such as MODIS, SeaWiFS, and MERIS, multiple ocean color scenes from a single sensor (i.e., GOCI) can be merged by averaging (Yang et al., 2012). Analysis of variance (ANOVA) was performed to validate the use of daily averaged values for the temporal composit of the GOCI chlorophyll concentration data. The goal is to statistically verify the existence of excess diurnal variations in the long-term GOCI-derived data which may invalidate the composit data. We collected chlorophyll concentration data from four locations (A, B, C, and D) for the time period of Jan-Dec, 2012, to observe

Table 1. ANOVAs for the GOCI chlorophyll concentration data from Jan. to Dec. 2012 in terms of hourly variations for the location points, A, B, C, and D in the Fig. 2.

Source groups	Sum of squres	Degree of freedom	Mean square	*F* value	Prob > *F*
A	0.449	7	0.064	0.607	0.750
B	4.331	7	0.619	0.393	0.907
C	12.147	7	1.735	1.068	0.384
D	0.371	7	0.053	1.143	0.336

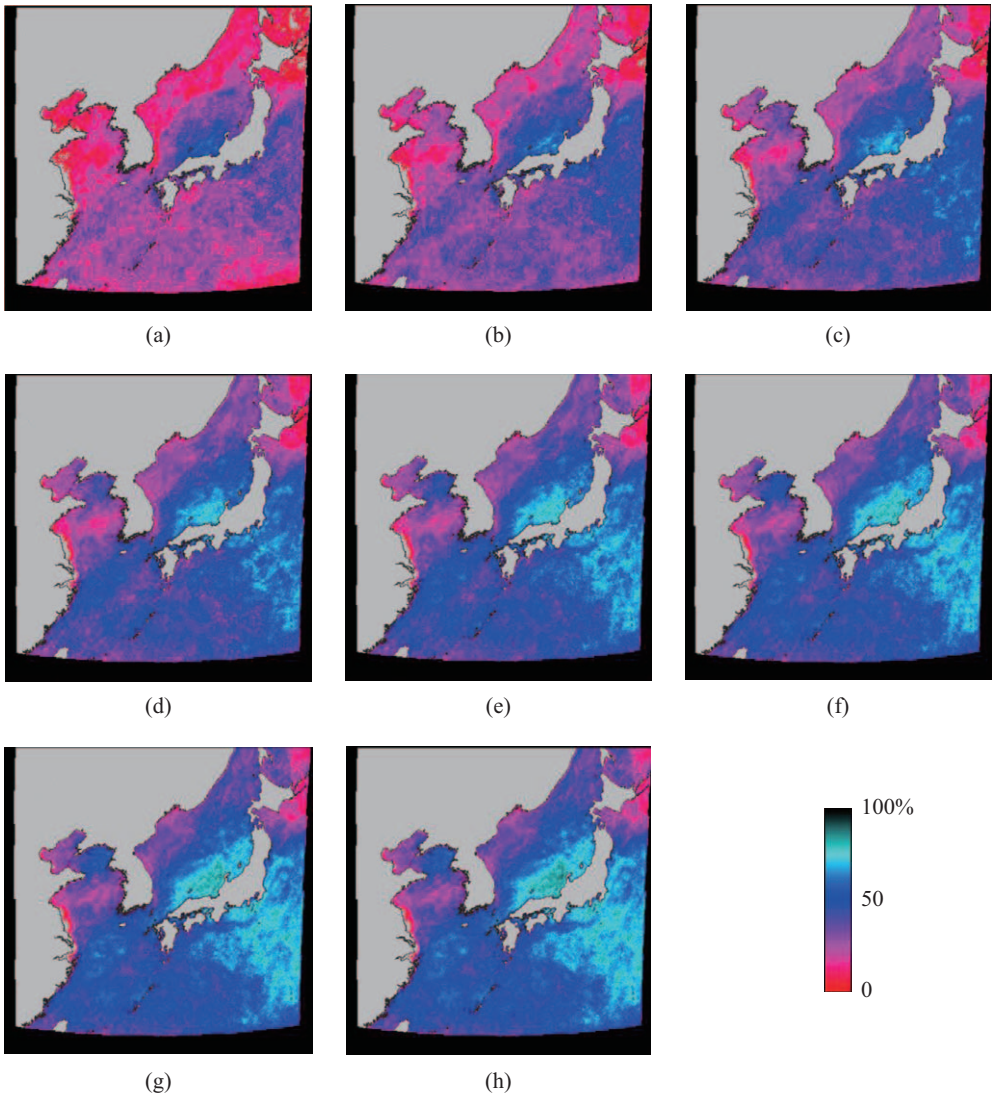

Fig. 6. Daily cumulative available rates, $CAR^j, j = (0, 1, \ldots, 7)$ every 9:30 (a), 9:30-10:30 (b), 9:30-11:30 (c), 9:30-12:30 (d), 9:30-13:30 (e), 9:30-14:30 (f), 9:30-15:30 (g), and 9:30-16:30 (h) local time during August 2012. The daily availability of GOCI data refers to the percentage of available observations of the eight observations during a day. For example, 50% implies that there is one available pixel for half a day.

the magnitude of diurnal variability (locations displayed in Fig. 2). The ocean chlorophyll 2-band (OC2) algorithm (O′Reilly et al., 1998; Moon et al., 2012) was applied to estimate chlorophyll concentration data after the GOCI standard atmospheric correction (Ahn et al., 2012). The region A indicates a sea area where oceanic eddies are formed frequently, B is a region that has a semidiurnal tide, C indicates a region that has extremely turbid water, and D is a relatively clear sea area.

The results are shown in Fig. 7 and Table 1. The results show that the null hypothesis that all the mean values from different hours are the same is not rejected (significance level, alpha = 0.05) for every location, suggesting that there is no significant

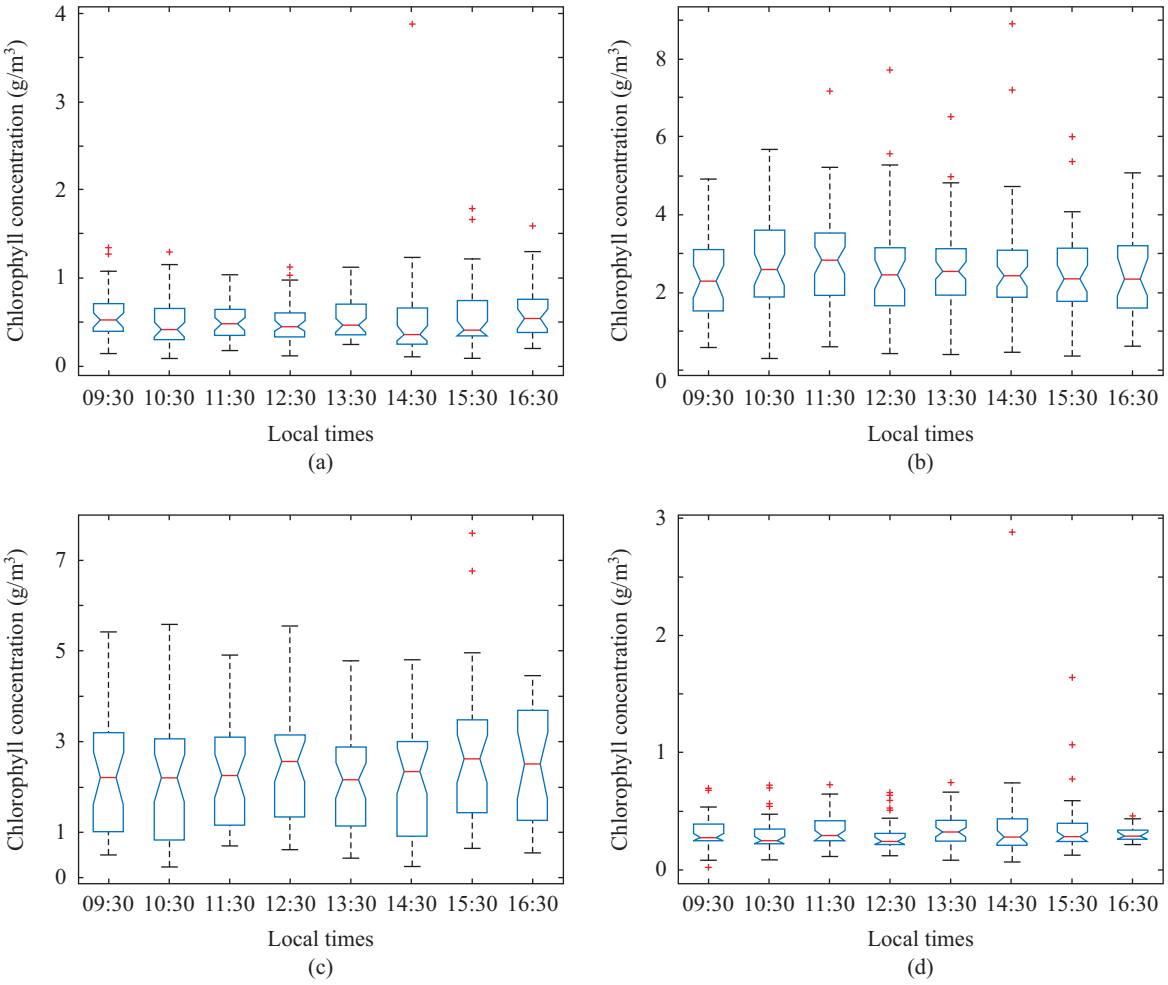

Fig. 7. Hourly variations of the GOCI chlorophyll concentration data from Jan. to Dec. 2012 for locations A-D((a)-(d)) in Fig. 2. On each graph, the central red line is the median, the edges of the blue box are the 25th and 75th percentiles, the black whiskers are max-min values, and red crosses are outliers on outside of three sigma in the normal distribution.

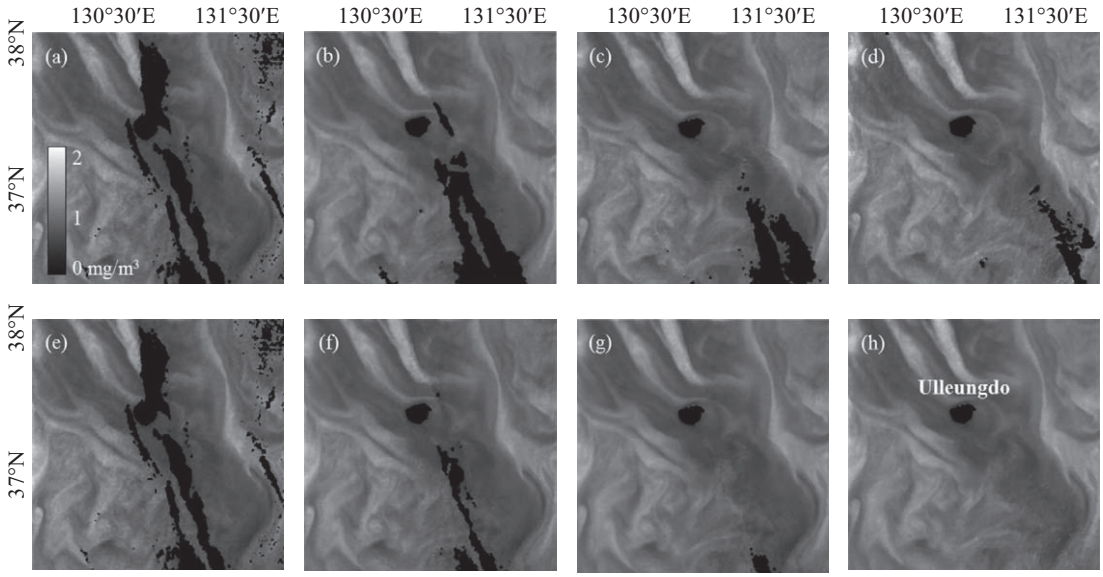

Fig. 8. Comparison between individual scenes at 10:30 (a), 11:30 (b), 12:30 (c), and 13:30 (d) and composite scenes merged by averaging at 10:30-10:30 (e), 10:30-11:30 (f), 10:30-12:30 (g), and 10:30-13:30 (h), for chlorophyll concentrations derived from GOCI on 3 April, 2013.

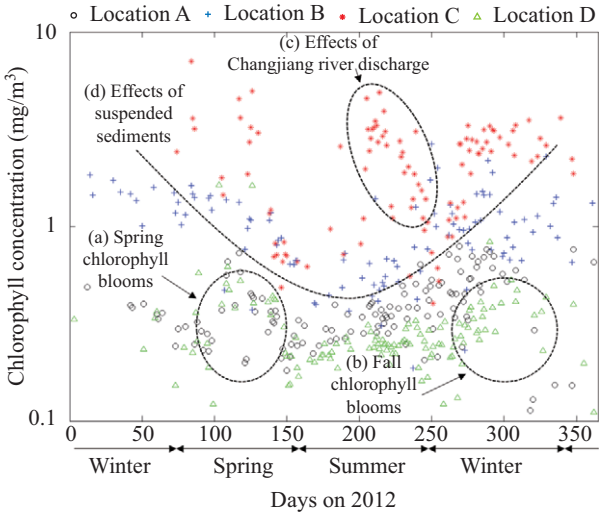

Fig. 9. Variations of daily composite scenes merged by averaging for chlorophyll concentrations derived from GOCI during 2012. (a) Spring chlorophyll blooms. (b) Fall chlorophyll blooms. (c) Effects of Changjiang river discharge from the East China. (d) Effects of the high suspended sediments around coastal areas during the winter season.

diurnal differences in those ocean areas from the long-term perspective. The result of the test supports the primary objective of the temporal composit which is to monitor long-term variability with maximum data availability.

Fig. 8 shows the availability improvements for composite scenes merged by averaging for chlorophyll concentrations derived from GOCI. It shows that visibility improves as the number of merged scenes increases. We expect that GOCI can be more efficiently utilized than the polar orbit remote sensors for monitoring a long-term (e.g., seasonal or annual) variability of ocen colors.

As shown in Fig. 9, we also performed an investigation to analyze variations of daily composite data of chlorophyll concentrations for four locations (Figs. 2(a)-(d)) during 2012. The result shows the various variability of chlorophyll concentrations. First, we could show well-known spring and fall chlorophyll blooms (Figs. 9(a) and (b)) (Yamada et al., 2004; Kim et al., 2007; Yoo and Park, 2009). In this sea area, spring and fall chlorophyll blooms begin few days after wind stress weakened (Kim et al., 2007). Also, we could find out that high chlorophyll blooms occur due to the Changjiang summer freshwater discharge (Fig. 9(c)) (Siswanto et al., 2008; Kim et al., 2009). As shown in Fig. 9(d), meanwhile, we could show that chlorophyll concentrations are over-estimated because of resuspension of sediments around the coastal areas during the winter season (Kiyomoto et al., 2001; Min et al., 2012; Yamaguchi et al., 2012).

Another important consideration is how the solar elevation angle (Bretagnon and Francou, 1988) impacts our masking algorithm (i.e., the KOSC standard atmospheric correction algorithm). The solar elevation angle means the altitude of the sun, the angle between the horizon and the center of the sun's disc.

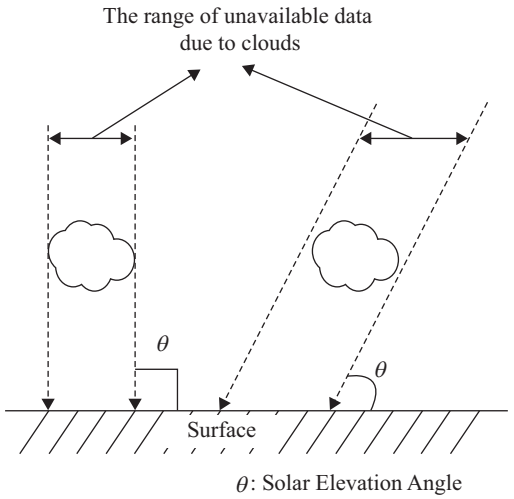

Fig. 10. A diagram for illustrating the variation of unavailable data range due to clouds as solar elevation angle

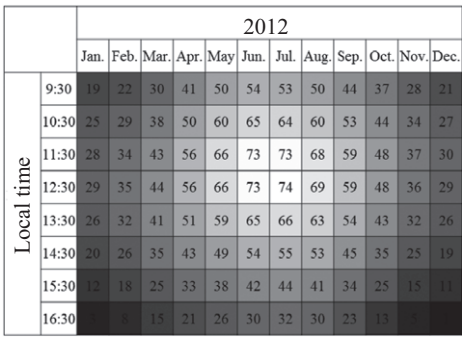

Local time	2012 Jan.	Feb.	Mar.	Apr.	May	Jun.	Jul.	Aug.	Sep.	Oct.	Nov.	Dec.
9:30	19	22	30	41	50	54	53	50	44	37	28	21
10:30	25	29	38	50	60	65	64	60	53	44	34	27
11:30	28	34	43	56	66	73	73	68	59	48	37	30
12:30	29	35	44	56	66	73	74	69	59	48	36	29
13:30	26	32	41	51	59	65	66	63	54	43	32	26
14:30	20	26	35	43	49	54	55	53	45	35	25	19
15:30	12	18	25	33	38	42	44	41	34	25	15	11
16:30		8	15	21	26	30	32	30	23	13	5	

(a) Solar elevation angle (°)

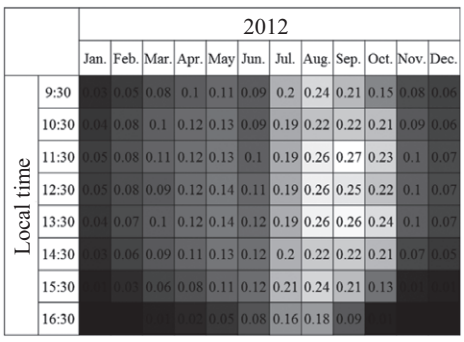

Local time	2012 Jan.	Feb.	Mar.	Apr.	May	Jun.	Jul.	Aug.	Sep.	Oct.	Nov.	Dec.
9:30	0.03	0.05	0.08	0.1	0.11	0.09	0.2	0.24	0.21	0.15	0.08	0.06
10:30	0.04	0.08	0.1	0.12	0.13	0.09	0.19	0.22	0.22	0.21	0.09	0.06
11:30	0.05	0.08	0.11	0.12	0.13	0.1	0.19	0.26	0.27	0.23	0.1	0.07
12:30	0.05	0.08	0.09	0.12	0.14	0.11	0.19	0.26	0.25	0.22	0.1	0.07
13:30	0.04	0.07	0.1	0.12	0.14	0.12	0.19	0.26	0.26	0.24	0.1	0.07
14:30	0.03	0.06	0.09	0.11	0.13	0.12	0.2	0.22	0.22	0.21	0.07	0.05
15:30	0.01	0.03	0.06	0.08	0.11	0.12	0.21	0.24	0.21	0.13	0.03	
16:30				0.02	0.05	0.08	0.16	0.18	0.09	0.01		

(b) Available Rate (*AR*)

Fig. 11. Changes of (a) the solar elevation angles and (b) the available rate (*AR*) for 2012 in terms of monthly and hourly averages.

Traditionally, it is well known that the unavailable data in the ocean color scene derived from the satellite should increase as the solar elevation angle decreases as shown in Fig. 10 (Minnis, 1989; Zhao and Di Girolamo, 2004; Ackerman et al., 2008).

The KOSC standard atmospheric correction algorithm is also affected by the solar elevation angle. The solar elevation angles and the *AR*s for 2012 are shown in Fig. 11, along with

monthly and hourly averages on the GOCI area. The variations in the *AR* and the solar elevation angle are similar to each other in terms of the changes in the local time. They tend to be high at mid-day (from 11:30 to 13:30 local time) and low in the morning (from 9:30 to 10:30 local time) and evening (from 14:30 to 16:30 local time). In terms of the monthly series, however, there are several differences between the variations in the *AR*s and the solar elevation angle, although the overall patterns of variation are similar. First, the *AR* tends to be high in autumn (from August to September), and the solar elevation angle tends to be high in summer (from June to August). Second, the *AR* in early summer (i.e., June) decreases due to the rainy season. These observations indicate that the available data in scenes of the ocean area in the Northeast Asian region are mainly affected by changes in the local time and the seasonal characteristics.

ACKNOWLEDGEMENTS

This research was supported by the "Research for applications of Geostationary Ocean Color Imager (GOCI)" and the "Development of the integrated data processing system for GOCI-II" funded by the Ministry of Ocean and Fisheries, Korea. This research was also supported by the "Operation in Korea Ocean Satellite Center" funded by the Korea Institute of Ocean Science and Technology (KIOST).

REFERENCES

Ackerman, S. A., R. E. Holz, R. Frey, E. W. Eloranta, B. C. Maddux and M. McGill (2008). Cloud detection with MODIS Part II: Validation. Journal of Atmospheric and Oceanic Technology 25, 1073-1086.

Ahn, J. H., Y. J. Park, J. H. Ryu and B. Lee (2012). Development of atmospheric correction algorithm for Geostationary Ocean Color Imager (GOCI). Ocean Science. Journal 47(3), 247-259.

Alvera-Azcarate, A., A. Barth, J. M. Beckers and R. H. Weisberg (2007). Multivariate reconstruction of missing data in sea surface temperature, chlorophyll and wind satellite fields. Journal of Geophysical Research-Oceans 112, 1-11 (C03008).

Bretagnon, P. and G. Francou (1988). Planetary Theories in Rectangular and Spherical Variables - Vsop-87 Solutions. Astronomy & Astrophysics 202, 309-315.

Campbell, J. W. and B. H. Stanford (1995). SeaWiFS Technical Report Series: Level-3 SeaWiFS Data Products: Spatial and Temporal Binning Algorithms: National Aeronautics and Space Administration, Goddard Space Flight Center.

Cho, S., Y. Ahn, J. Ryu, G. Kang and H. Youn (2010). Development of Geostationary Ocean Color Imager (GOCI). Korean. Journal of Remote Sensing 26, 157-165.

Choi, J. K., Y. J. Park, J. H. Ahn, H. S. Lim, J. Eom and J. H. Ryu (2012). GOCI, the world's first geostationary ocean color observation satellite, for the monitoring of temporal variability in coastal water turbidity. Journal of Geophysical Research: Ocean 117(C09004), 1-10.

Cihlar, J. and J. Howarth (1994). Detection and Removal of Cloud Contamination from Avhrr Images. IEEE Transactions on Geoscience and Remote Sensing 32, 583-589.

Esaias, W. E., M. R. Abbott, I. Barton, O. B. Brown, J. W. Campbell, K. L. Carder, D. K. Clark, R. H. Evans, F. E. Hoge, H. R. Gordon, W. M. Balch, R. Letelier and P. J. Minnett (1998). An overview of MODIS capabilities for ocean science observations. IEEE Transactions on Geoscience and Remote Sensing 36, 1250-1265.

Han, H., J. Ryu and Y. Ahn (2010). Development the Geostationary Ocean Color Imager (GOCI) Data Processing System (GDPS). Korean Journal of Remote Sensing 26, 239-249.

He, R. Y., R. H. Weisberg, H. Y. Zhang, F. E. Muller-Karger and R.W. Helber (2003). A cloud-free, satellite-derived, sea surface temperature analysis for the West Florida Shelf. Geophysical Research Letters 30, 1-5 (OCE 4).

Kang, G., S. Kang, S. Yong, J. Kim, Y. Chang and H. Youn (2004). Korea geostationary ocean color imager (KGOCI). In Proceedings of IEEE International Geoscience and Remote Sensing Symposium (IGARSS 04) 5, 3261-3263.

Kim, H., H. Yamaguchi, S. Yoo, J. Zhu, K. Okamura, Y. Kiyomoto, K. Tanaka, S. Kim, T. Park, I. S. Oh and J. Ishizaka (2009). Distribution of Changjiang Diluted Water Detected by Satellite Chlorophyll-a and Its Interannual Variation during 1998-2007. Journal of Oceanography 65, 129-135.

Kim, H., S. Yoo and I. S. Oh (2007). Relationship between phytoplankton bloom and wind stress in the sub-polar frontal area of the Japan/East Sea. Journal of Marine Systems 67, 205-216.

Kiyomoto, Y., K. Iseki and K. Okamura (2001). Ocean Color satellite imagery and shipboard measurements of chlorophyll a and suspended particulate matter distribution in the East China Sea. Journal of Oceanography 57, 37-45.

Maritorena, S., O. H. F. d'Andon, A. Mangin and D. A. Siegel (2010). Merged satellite ocean color data products using a bio-optical model: Characteristics, benefits and issues. Remote Sensing of Environment 114, 1791-1804.

Maritorena, S. and D. A. Siegel (2005). Consistent merging of satellite ocean color data sets using a bio-optical model. Remote Sensing of Environment 94, 429-440.

McClain, C. R., G. C. Feldman and S. B. Hooker (2004). An overview of the SeaWiFS project and strategies for producing a climate research quality global ocean bio-optical time series. Deep-Sea Research Part Ii-Topical Studies in Oceanography 51, 5-42.

Min, J., J. Ryu, S. Lee and S. Son (2010). Monitoring of suspended sediment variation using Landsat and MODIS in the Saemangeum coastal area of Korea. Marine Pollution Bulletin 64, 382-390.

Minnis, P. (1989). Viewing zenith angle dependence of cloudiness determined from coincident goes east and goes west data. Journal of Geophysical Research-Atmospheres 94, 2303-2320.

Moon, J. E., Y. J. Park, J. H. Ryu, J. K. Choi, J. H. Ahn, J. E. Min, Y. B. Son, S. J. Lee, H. J. Han and Y. H. Ahn (2012). Initial validation of GOCI water products against in situ data collected around Korean Peninsula for 2010-2011. Ocean Science Journal 47(3), 261-277.

Oh, K., J. Lee, S. Lee and I. Pang (2014). Intrusion of low-salinity water into the yellow sea interior in 2012. Ocean Science Journal 49(4), 343-356.

O'Reilly, J. E., S. Maritorena, B. G. Mitchell, D. A. Siegel, K. L. Carder, S. A. Garver, M. Kahru and C. McClain (1998). Ocean color chlorophyll algorithms for SeaWiFS. Journal of Geophysical Research-Oceans 103(C11), 24937-24953.

Pottier, C., V. Garcon, G. Larnicol, J. Sudre, P. Schaeffer and P.Y. Traon (2006). Merging SeaWiFS and MODIS/Aqua ocean color data in North and Equatorial Atlantic using weighted averaging and objective analysis. IEEE Transactions on Geoscience and Remote Sensing 44, 3436-3451.

Rast, M., J. L. Bezy and S. Bruzzi (1999). The ESA Medium Resolution Imaging Spectrometer MERIS - a review of the instrument and its mission. International Journal of Remote Sensing 20, 1681-1702.

Roy, D. P., P. Lewis, C. B. Schaaf, S. Devadiga and L. Boschetti (2006). The global impact of clouds on the production of MODIS bidirectional reflectance model-based composites for terrestrial monitoring. IEEE Geoscience and Remote Sensing Letters 3, 452-456.

Ruddick, K. G., F. Ovidio and M. Rijkeboer (2000). Atmospheric correction of SeaWiFS imagery for turbid coastal and inland waters. Applied Optics 39, 897-912.

Ryu, J. H., H. J. Han, S. Cho, Y. J. Park and Y. H. Ahn (2012). Overview of geostationary ocean color imager (GOCI) and GOCI data processing system (GDPS). Ocean Science Journal 47, 223-233.

Siswanto, E., H. Nakata, Y. Matsuoka, K. Tanaka, Y. Kiyomoto, K. Okamura, J. Zhu and J. Ishizaka (2008). The long-term freshening and nutrient in-

creases in summer surface water in the northern East China Sea in relation to Changjiang discharge variation. Journal of Geophysical Research-Ocean 113(C10030), 1-13.

Wang, M. H. and W. Shi (2006). Cloud masking for ocean color data processing in the coastal regions. IEEE Transactions on Geoscience and Remote Sensing 44, 3196-3205.

Yamada, K., J. Ishizaka, S. Yoo, H. C. Kim and S. Chiba (2004). Seasonal and interannual variability of sea surface chlorophyll a concentration in the Japan/East Sea (JES). Progress in Oceanography 61, 193-211.

Yamaguchi, H., H. Kim, Y. B. Son, S. W. Kim and K. Okamura, Y. Kiyomoto, J. Ishizaka (2012). Seasonal and summer interannual variations of SeaWiFS chlorophyll a in the Yellow Sea and East China Sea. Progress in Oceanography 105, 22-29.

Yang, H., J. H. Ahn, H. J. Han, J. H. Ryu and Y. J. Park (2012). How cloud-free areas increase with eight times observations of geostationary ocean color imager. In Proceeding of International Symposium on Remote Sensing (ISRS 2012).

Yang, H., J. K. Choi, Y. J. Park, H. J. Han and J. H. Ryu (2014). Application of the Geostationary Ocean Color Imager (GOCI) to estimates of ocean surface currents. Journal of Geophysical Research: Ocean 119(6), 3988-4000.

Yang, H., E. Oh, J. K. Choi, Y. J. Park and H. J Han (2016). Application of Geostationary Ocean Color Imager Data to the extraction of ocean fronts. Remote Sensing Letters 7(5), 456-465.

Yoo, S. and J. Park (2009). Why is the southwest the most productive region of the East Sea/Sea of Japan? Journal of Marine Systems 78(2), 301-315.

Zhao, G. Y. and L. D. Girolamo (2004). A cloud fraction versus view angle technique for automatic in-scene evaluation of the MISR cloud mask. Journal of Applied Meteorology 43, 860-869.